The Cryosphere Discuss., doi:10.5194/tc-2016-248, 2016
Manuscript under review for journal The Cryosphere
Published: 14 November 2016

The Cryosphere Discussions
Open Access
EGU

Regional Greenland Accumulation Variability from Operation IceBridge Airborne Accumulation Radar

Lewis, Gabriel[1]; Osterberg, Erich[1]; Hawley, Robert[1]; Whitmore, Brian.[1].; Marshall, Hans Peter[2]

[1]Department of Earth Sciences, Dartmouth College, Hanover, NH, USA
[2]Geosciences Department, Boise State University, Boise, ID, USA

Correspondence to: Gabriel Lewis (Gabriel.M.Lewis.GR@dartmouth.edu)

Abstract. The mass balance of the Greenland Ice Sheet (GIS) in a warming climate is of critical interest to scientists and the general public in the context of future sea-level rise. An improved understanding of temporal and spatial variability of snow accumulation will reduce uncertainties in GIS mass balance models and improve projections of Greenland's contribution to sea-level rise, currently estimated at 0.089 ± 0.03 m by 2100. Here we analyze 25 NASA Operation IceBridge Accumulation Radar flights totaling >17,700 km from 2013-2014 to determine snow accumulation in the GIS dry snow and percolation zones over the past 100-300 years. IceBridge accumulation rates are calculated and used to validate accumulation rates from three regional climate models. Averaged over all 25 flights, the RMS difference between the models and IceBridge accumulation is between 0.037 ± 0.022 and 0.064 ± 0.033 m w.e. a^{-1}, although each model shows significantly larger differences from IceBridge accumulation on a regional basis. In the central northern region, for example, the Regional Atmospheric Climate MOdel (RACMO2) underestimates by 26.9 ± 4.5%, while in the southeast region the Modèle Atmosphérique Régional (MAR) overestimates by as much as 35.5 ± 6.8%. Our results indicate that these regional differences between model and IceBridge accumulation are large enough to significantly alter GIS surface mass balance estimates. Empirical orthogonality function analysis suggests that the first two principal components account for 33% and 18% of the variance and correlate with the Atlantic Multidecadal Oscillation (AMO) and wintertime North Atlantic Oscillation (NAO), respectively. From 1976-2014 accumulation increased over most of the ice sheet's interior, consistent with the response to a positive AMO trend over this period. Regions that disagree strongest with climate models are those in which we have the fewest IceBridge data points, requiring additional *in situ* measurements to verify model uncertainties.

1. Introduction

Assessing the stability of the Greenland Ice Sheet (GIS) in a warming world is crucial for predicating future global sea-level rise and its societal and economic impacts (Dumont et al., 2014; IPCC, 2014). The mass balance of the GIS has been decreasing over the 1988-2016 period, with a conservative estimate of ice sheet mass loss of 272 ± 24 Gt a^{-1} (Khan et al., 2015; Sasgen et al., 2012; Shepherd, 2012), or an equivalent

The Cryosphere Discuss., doi:10.5194/tc-2016-248, 2016
Manuscript under review for journal The Cryosphere
Published: 14 November 2016

global sea-level rise of ~0.7 ± 0.2 mm a^{-1} (Ettema et al., 2009; Helm et al., 2014). The dominant mass loss process for the GIS has changed from ice discharge (i.e. calving) to surface mass balance (SMB) since the mid-1990s (van den Broeke et al., 2009). SMB is one of the largest sources of error in estimates of the ice sheet's total mass balance (van den Broeke et al., 2009) due to complex relationships between accumulation variability and surface melt runoff (Dumont et al., 2014; McConnell et al., 2000).. GIS snow accumulation varies spatially in response to surface topography (e.g. Hawley et al., 2014), wind redistribution (Déry and Yau, 2002), and preferred modes of climate variability like the North Atlantic Oscillation (NAO; e.g. Wong et al., 2015) and Atlantic Multidecadal Oscillation (AMO; e.g. Mernild et al., 2014) that affect certain regions of the ice sheet more than others. Accumulation also varies through time largely in response to temporal changes in these climate modes (Mernild et al., 2014). Ice cores accurately record temporal accumulation changes at point locations (Banta and McConnell, 2007; McConnell et al., 2000; Mosley-Thompson et al., 2001), but are too sparse to capture the full spatial variability of GIS accumulation, especially in the southeast. Further, many Greenland ice cores were collected during the 1990s or earlier, prior to the recent acceleration of GIS mass loss (Box, 2013). An updated and more spatially distributed GIS accumulation dataset is needed to evaluate recent precipitation trends and to validate GIS SMB estimates from regional climate models over recent decades of increased mass loss.

Here we develop a record of GIS snow accumulation over a large portion of the GIS interior from 1712 to 2014 AD using the airborne NASA Operation IceBridge Accumulation Radar. Airborne and ground-based radars have been used to map spatial patterns of accumulation in Greenland over decadal (Hawley et al., 2014; Miège et al., 2013) and annual resolutions (Koenig et al., 2016; Medley et al., 2013). Operation IceBridge collected Accumulation Radar data from 2009-2014, and it has been used in several studies (Forster et al., 2014; Leuschen et al., 2011; Medley et al., 2013) to calculate local accumulation. We examine Accumulation Radar data from every IceBridge flight across the Greenland interior during the 2013-2014 seasons to measure accumulation rates over the majority of the dry and upper percolation zones.

Regional climate models (RCMs) and reanalysis products provide spatially and temporally comprehensive estimates of accumulation at ice-sheet scales. The magnitude of mesoscale model uncertainty can be as large as the natural variability, or larger in areas with sparse *in situ* measurements like ice cores, potentially obscuring climate fluctuations with random error (Burgess et al., 2010; Box et al., 2006). Current RCM analyses of GIS SMB from 1960-2008 differ by as much as 130 Gt a^{-1} across the ice sheet, with especially large differences in the southern (80.1 Gt a^{-1}) and northwestern (40.4 Gt a^{-1}) drainage basins (Vernon et al., 2013). Many of the variables included in these models are validated with snow pits and ice cores, such as the 1997-1998 Program for Regional Climate Assessment (PARCA) ice core campaign (Mosley-Thompson

The Cryosphere Discuss., doi:10.5194/tc-2016-248, 2016
Manuscript under review for journal The Cryosphere
Published: 14 November 2016

et al., 2001), which predates the recent period of accelerated surface melting in Greenland (McGrath et al., 2013). We compare our IceBridge accumulation data with outputs from three RCMs to pinpoint their areas of highest uncertainty: (1) the Regional Atmospheric Climate MOdel (RACMO2; Ettema et al., 2009), (2) the Pennsylvania State University – National Center for Atmospheric Research Fifth-Generation Mesoscale Model (Polar MM5; Burgess et al., 2010), and (3) the Modèle Atmosphérique Régional (MAR; Fettweis et al., 2012). We further use principle component analyses to evaluate the dominant climate forcing mechanisms driving regional GIS precipitation trends.

2. Methods

2.1. Accumulation radar

We calculate a spatially continuous record of accumulation along 17,730 km of NASA Operation IceBridge Accumulation Radar flights (hereafter "IceBridge accumulation"). Operation IceBridge was designed to bridge the gap in polar observations between the Ice, Cloud, and Land Elevation Satellite (ICESat; 2003-2009) and ICESat-2, which is scheduled to launch in 2017. Laser altimeters, 4-5 radars with different frequencies, a gravimeter, and a magnetometer are mounted on NASA's P-3B and DC-8 airplanes, which conduct airborne surveys in both the Arctic and Antarctic each spring.

The IceBridge Accumulation Radar captures a continuous electromagnetic profile of the top few hundred meters of the ice sheet, displaying distinct internal reflecting horizons (IRHs) that can be traced for hundreds of kilometers (Leuschen et al., 2011). The Accumulation Radar operates in the 600-900 MHz range and has an average vertical resolution of 0.28 m in snow/firn, which is fine enough to resolve IRHs that have been shown to represent isochrones (Medley et al., 2013; Rodriguez-Morales et al., 2014; Spikes et al., 2004; Hawley et al., 2014). The average distance between radar traces is 16 m, which we then average over 10 adjacent traces to increase the signal-to-noise ratio. The position of each trace is known from differential GPS receivers mounted on the aircraft. We do not perform any time variable gain or additional filtering on the IceBridge accumulation data. Depending on signal attenuation within the snowpack, IRHs can be traced to a depth of 50-150 m and provide accumulation records over the past 100-300 years (Figure 1). For areas with high attenuation (i.e. shallow penetration of the radar signal), such as those at relatively lower elevations (e.g. below ~2500 m), we calculate accumulation results for 1921-2014. Where the signal is less attenuated higher on the ice sheet, we calculate accumulation over the 1712-2014 time period (Figure 2).

The Cryosphere Discuss., doi:10.5194/tc-2016-248, 2016
Manuscript under review for journal The Cryosphere
Published: 14 November 2016

2.2. Depth-age scales and density profiles

To calculate accumulation rates using ice penetrating radar, one must know the amount of snow mass between IRHs and their relative ages. The mass between IRHs is a function of the depth-age scale, travel time-depth conversion rate, and firn or ice density. We obtain both the density profile and depth-age scale from two dated ice cores collected at Summit Station (Mary Albert, personal communication, 2015; Cole-Dai et al., 2009).

We calibrate a Herron-Langway (1980) depth-density model at Summit using data from both ice cores, and then use the calibrated model parameters to estimate density profiles elsewhere in our study region. Input parameters for this model include satellite derived mean annual temperature (Hall et al., 2012), modelled accumulation (Burgess et al., 2010), and an estimate of surface snow density from field measurements along ground traverses and at shallow firn cores. Since we are using the density profile to calculate accumulation based, in part, on modelled accumulation, the result could be seen to be circular. However, our results are largely insensitive to changes in this modelled accumulation input because accumulation estimates are minimally affected by input variations to the Herron-Langway model. For example, adjusting input accumulation and surface density by ±5% results in <1% change in the calculated accumulation rates.

2.3. Travel-time to depth conversion

We convert the radar travel time to depth by iteratively multiplying the velocity of the electromagnetic wave by the signal's travel time to each IRH. The electromagnetic speed of the radar wave, v (m s^{-1}), is calculated from the dielectric permittivity, ε_r (dimensionless), and the speed of light in a vacuum, c (3×10^8 m s^{-1}), from

$$v = \frac{c}{\sqrt{\epsilon_r}} \quad \textbf{(Equation 1).}$$

In turn, the dielectric permittivity is calculated from the density, ρ (g m^3), of snow and ice at depth for each radar trace (following Kovacs et al., 1995) by

$$\epsilon_r = (1.0 + 0.845 * \rho)^2 \quad \textbf{(Equation 2).}$$

The snow surface reflection is readily identified in each radar profile from the large signal amplitude. We then calculate the depth for each subsequent radar sample in the profile using the radar travel time and velocity profile from Eqn. 1 and 2, following Hawley et al. (2014).

The Cryosphere Discuss., doi:10.5194/tc-2016-248, 2016
Manuscript under review for journal The Cryosphere
Published: 14 November 2016

2.4. Internal reflecting horizons

We manually select 19 clear, strong IRHs to consistently trace from Summit Station towards the NNW and SW along two main flight paths (April 5 and May 2, 2014, respectively; Figure 1). When a layer appears to bifurcate due to changes in accumulation, we continue to trace the layer based on the trajectory of surrounding IRHs. Horizons are not traced in areas where the signal-to-noise ratio made them too difficult to discern.

Internal reflecting horizons for the other 23 flights in this study are traced from crossover locations with the two main flight paths. Wherever possible, we trace IRHs outwards from crossover locations along the two main flight paths to locations where those traced layers cross another flight path. Whenever we have accumulation differences at crossover locations larger than our accepted error, we retrace IRHs to determine which layers are incorrectly traced.

2.5. Accumulation calculations and uncertainty

Finally, we calculate snow accumulation using the ice core depth-age scales, modelled depth-density profiles, and traced IRHs. We calculate the water equivalent accumulation, $\dot{b}$ (m w.e. a^{-1}), between adjacent IRHs from the depth, z (m) and age, t (year), of each layer, the density, ρ (kg m^{-3}), between layers, and the density of water, ρ_w (1000 kg m^{-3}):

$$\dot{b} = \frac{1}{t_2 - t_1} \int_{z_1}^{z_2} \frac{\rho(z)}{\rho_w} \partial z \qquad \textbf{(Equation 3).}$$

Accumulation uncertainty can arise from independent errors in tracing IRHs, errors from incorrectly dating the ice core, and/or errors in the densities used for converting from separation distance to water equivalent accumulation.

To reduce tracing errors, two authors separately retraced each IRH along the two main flights paths four times each. Close inspection of the IRHs reveals that the peaks defining IRHs are within ±2 radar samples (within ±0.557 m), and incorrectly jumping to the next layer would result in an error of at most ±5 samples (within ±1.39 m). Our average epoch between IRHs is 16.7 years, which corresponds to a maximum error of ~±0.083 m a^{-1}.

We take uncertainty in dating the Summit ice cores to be ±1% for the top 100 years, ±2% for 100-200 years ago, and ±3% for 200-300 years ago. The oldest isochrones traced in this study are dated to 1712, which suggests a maximum error of 3% using a 2007 Summit Station ice core. At the lowest accumulation

The Cryosphere Discuss., doi:10.5194/tc-2016-248, 2016
Manuscript under review for journal The Cryosphere
Published: 14 November 2016

locations, the smallest distance between layers is 0.26 m w.e. over an epoch of 5.18 years. This gives an uncertainty in accumulation due to dating of ~±0.03 m w.e. a^{-1}.

The error associated with measuring density using similar techniques has been estimated to be 1.4% (Karlöf et al., 2005). However, following Hawley et al. (2014) we assume that our measurements have an error of up to twice this large, corresponding to a maximum accumulation error of ±0.014 m w.e. a^{-1}.

The three error sources are all random, non-systematic, and thus can be assumed to be non-additive (following Hawley et al., 2014). Over the extent of the dataset we can assume that the errors are not correlated, thus we estimate accumulation uncertainty for all causes at ±0.127 m w.e. a^{-1} for any single epoch. Due to the random and non-systematic nature of these errors, we can assume that they are unlikely to contribute to a regional or temporal accumulation bias. To calculate uncertainty for accumulation averaged over multiple epochs, we divide our uncertainty by the square root of the number of traced layers at that location

2.6. Model comparison

We compare our IceBridge accumulation results with annual outputs from Polar MM5 (1958-2008; Burgess et al., 2010), MAR (1958-2013; Fettweis et al., 2012), and RACMO2 (1958-2014; Ettema et al., 2009). Grid cell sizes for these model outputs are 24 km, 25 km, and 11 km, respectively. Since accumulation can be bilinearly interpolated over the distance of these grid cells without significant loss of detail, we choose to compare IceBridge accumulation with bilinearly interpolated model grid output to compare accumulation at corresponding spatial locations (Box et al., 2003)

Additionally, we compare our IceBridge accumulation with an accumulation map kriged from 295 ice cores and 20 coastal weather stations (Bales et al., 2009; hereafter "Bales09"). While this map estimates accumulation over the time domain of the oldest ice cores, we choose to compare IceBridge accumulation with the highest accuracy accumulation estimates from 1950-2000, which include weather stations and recent ice cores.

The Cryosphere Discuss., doi:10.5194/tc-2016-248, 2016
Manuscript under review for journal The Cryosphere
Published: 14 November 2016

3. Results and discussion

3.1. IceBridge accumulation rates

IceBridge accumulation patterns are consistent with observed large-scale spatial patterns from ice cores and snow pits (Bales et al., 2009), with high accumulation rates in the southeast and southwest and lower accumulation rates in the northeast and at higher elevations of the ice sheet interior (Figure 3). The number of traceable layers is highest towards the interior of the ice sheet and lowest in warmer areas towards the coast and in the south, where enhanced surface melt attenuates the radar signal and reduces the density gradients that produce IRHs (Figure 2).

We assess the internal consistency of IceBridge accumulation by comparing the accumulation at 87 locations where IceBridge flight paths cross one another (hereafter "crossover points"). Differences at crossover points are most likely due to errors in layer picking where isochrones become difficult to detect or distinguish. There are no spatial or temporal patterns in accumulation differences at crossover points over the dataset. Moreover, the differences are normally distributed with a mean of 0.013 ± 0.015 m w.e. a^{-1} ($n = 1272$), and all crossover points fall within our calculated uncertainty of 0.127 m w.e. a^{-1} over each individual epoch (Figure 4).

3.2. Validation with in-situ measurements

Accumulation rates derived from ice cores collected at Camp Century, D3, and D4 (see Figure 2 for locations) correspond closely with our IceBridge accumulation rates, matching their long-term mean and tracking their decadal variability (Figure 5). Additionally, we compare IceBridge accumulation to the NASA-U, NEEM, D5, and PARCA ice cores over the temporal domain of each core (Table 1). IceBridge accumulation rates are statistically indistinguishable from each of these cores at a $p < 0.05$ confidence level using a Student's t-test.

In Figure 6 we compare IceBridge accumulation to snowpit measurements at station T-31 on the Expédition Glaciologique Internationale au Groenland (EGIG) traverse (Fischer et al., 1995; Hurbertus Fischer, personal communication., 2015), and to accumulation rates calculated at this location from the Airborne SAR/Interferometric Radar Altimeter System (ASIRAS; Overly et al., 2016) (see Figure 2 for location). IceBridge accumulation rates are statistically indistinguishable ($p < 0.05$) from the snowpit measurements and ASIRAS accumulation results (Figure 6).

The Cryosphere Discuss., doi:10.5194/tc-2016-248, 2016
Manuscript under review for journal The Cryosphere
Published: 14 November 2016

3.3. Comparison to modelled accumulation

We compare IceBridge accumulation to RCM SMB results along the length of each flight across the GIS. IceBridge accumulation is averaged over 1957-2014 to compare with averaged Polar MM5 (1958-2008), MAR (1958-2013), and RACMO2 (1958-2014). An example of this comparison along a single flight (B-B'-B'' in Figure 2) is shown in Figure 7. Differences between the IceBridge accumulation and RCM output are spatially heterogeneous along the flight path, varying in both location and magnitude depending on the RCM. Averaged over the entire length of the flight, Polar MM5 underestimates accumulation by 0.001 ± 0.010 m w.e. a^{-1}, MAR overestimates by 0.023 ± 0.009 m w.e. a^{-1}, RACMO2 underestimates by 0.030 ± 0.011 m w.e. a^{-1}, and Bales09 overestimates by 0.007 ± 0.014 m w.e. a^{-1} (Figure 7). In addition, the high spatial resolution of our dataset shows significant accumulation variability not captured in model outputs.

The model output and IceBridge accumulation time domains do not match identically, but these minor differences do not significantly affect our results. The largest time domain discrepancy is with the Polar MM5 comparison, where model output is averaged from 1958-2008 and IceBridge accumulation is averaged from 1957-2014. The top panel of Figure 7 shows Polar MM5 output averaged from 1958-2008 compared to IceBridge accumulation averaged from 1957-2004. The difference between IceBridge averaged over 1957-2014 and IceBridge averaged over 1957-2004 along this flight is 0.00096 ± 0.0021 m w.e. a^{-1}, well within calculated error.

Next, we compute the magnitude and percent differences between RCM output and IceBridge accumulation over the entire domain of this data set. Averaged over all 25 flights, the RMS difference between the models and IceBridge accumulation is 0.037 ± 0.022 m w.e. a^{-1} for Polar MM5, 0.043 ± 0.018 m w.e. a^{-1} for RACMO2, and 0.064 ± 0.033 m w.e. a^{-1} for MAR. These average RMS errors are remarkably small, but Figure 8 shows considerably larger model-specific regional differences between IceBridge accumulation and RCM output.

Inspection of Figure 8 reveals that Polar MM5 and MAR have the smallest differences from IceBridge accumulation along the high central divide of the ice sheet, with larger differences (in both magnitude and percent) lower on the ice sheet towards the coasts. In contrast, RACMO2 underestimates throughout the whole region (Figure 8), with larger differences along the central divide and smaller differences towards both the east and west coast.

The Cryosphere Discuss., doi:10.5194/tc-2016-248, 2016
Manuscript under review for journal The Cryosphere
Published: 14 November 2016

We divide the Greenland ice Sheet into six major drainage basins following Vernon et al. (2013) to evaluate and discuss the spatial differences between model and IceBridge accumulation. Table 2 shows both percent and magnitude differences between the models and 1957-2014 averaged IceBridge accumulation in each of the six drainage basins. Statistically significant differences ($p < 0.05$) are highlighted in bold.

Both RACMO2 and MAR accumulation are significantly different from IceBridge accumulation in basin A, the northern basin with generally low accumulation rates. Averaged over all 135 data points in this basin, RACMO2 underestimates by 15.0 ± 4.0%, while MAR overestimates by 14.3 ± 4.7% (Table 2). Averaged across basin B in the northeast, RACMO2 is the only model with a statistically significant difference from IceBridge accumulation, underestimating by 26.9 ± 4.5%. Basin C in the east has the largest difference between models and IceBridge accumulation, where MAR overestimates by 35.5 ± 6.8% and Polar MM5 underestimates by 8.9 ± 5.9%.

Basin D in the southeast has very little coverage by our data, but has large differences between model and IceBridge accumulation. RACMO2 underestimates by 10.1 ± 1.9% while MAR overestimates by 27.6 ± 9.2%. Koenig et al. (2016) similarly found that MAR overestimates accumulation in the SE region for the years 2009-2011 in comparison to IceBridge snow radar accumulation rates. Averaged across basin E, there are no statistically significant differences between IceBridge accumulation and any of the RCMs used in this study. Likewise, Vernon et al. (2013) finds little difference in basin E between the climate models used in that study. On the other hand, all three RCMs underestimate accumulation in basin F, with statistically significant differences for Polar MM5 (11 ± 5.2%) and RACMO2 (17.7 ± 6.4%). Figure 8 shows that the differences are particularly large near Camp Century (see Figure 2 for reference), where Polar MM5 underestimates by 18.9 ± 5.8% and MAR overestimates by 21.2 ± 7.5%.

In summary, the RCMs do an excellent job of calculating accumulation averaged over basin E, but there are larger differences between model and IceBridge accumulation in basins C and D, where we also have the fewest data points. Areas where RCM and IceBridge accumulation differ the most are concurrent with areas without many *in situ* measurements (e.g. in the southeast), where ice cores that were collected several decades ago (e.g. NASA-U, Camp Century). Additional field measurements would be beneficial to validate our IceBridge accumulation measurements in these data poor regions.

Averaged across all 25 flights, the Bales accumulation model kriged from ice core and snow pit measurements differs from averaged 1957-2014 IceBridge accumulation by 0.037 ± 0.023 m w.e. a^{-1}

The Cryosphere Discuss., doi:10.5194/tc-2016-248, 2016
Manuscript under review for journal The Cryosphere
Published: 14 November 2016

(Figure 9). There are no statistically significant differences in any of the six drainage basins (Table 2), although differences are also largest in areas with sparse *in situ* measurements.

Basins B, E and F have sufficient data coverage to extrapolate over these basins' spatial domain to estimate the model uncertainty on their SMB estimates. We obtain total model uncertainty (in GT a^{-1}) by multiplying the percent difference in Table 2 by the annual regional SMB in each basin over 1961-1990 (Table 3 from Vernon et al., 2013). For basins B, E, and F, MAR differs by a combined total of -10.4 to 23.4 Gt a^{-1}, RACMO2 underestimates by 17.73 to 42.95 GT a^{-1}, and Polar MM5 underestimates by 6.58 to 30.77 Gt a^{-1}. Given a modelled GIS SMB of 363 ± 89 GT a^{-1} (Vernon et al., 2013), the uncertainties in these three basins represent a total SMB difference of -2.87% to 6.44% (MAR), an underestimation of 4.88% to 11.83% (RACMO2) or an underestimation of 1.81% to 8.48% (Polar MM5). Today, it would take 360 GT of ice mass loss to raise global sea level by 1 mm. Thus, the combined RACMO2 SMB underestimation from basins B, E, and F would represent 0.049 to 0.119 mm a^{-1} of less sea level rise from Greenland.

3.4. IceBridge accumulation temporal trends

Using our IceBridge accumulation record across 17,700 km of flight paths over the past 300 years, we can analyze spatiotemporal trends in snow accumulation. We perform an empirical orthogonality function (EOF) analysis on the dataset to evaluate temporal changes in accumulation and assess potential atmospheric forcing mechanisms (Figure 10). We limit our EOF analysis to 1889-2014 to capture the maximum spatial variability since layers older than 1889 are difficult to trace in the southern region (see Figure 2). We find that EOF1 and EOF2 represent most of the variance within the dataset, explaining 33% and 19% of the variance, respectively.

The EOF1 time series has a statistically significant correlation with the 1899-2014 annually averaged Atlantic Multidecadal Oscillation (AMO) index ($r = 0.60$, $p < 0.04$), the wintertime (DJF) AMO ($r = 0.55$, $p < .05$), and the springtime (MAM) AMO ($r = 0.56$, $p < 0.05$). These correlations indicate a major influence of the AMO on Greenland precipitation. Mernild et al. (2014) similarly found a significant positive relationship between the AMO and a composite Greenland ice core precipitation record from 1890-2000. Figure 10a indicates that while the majority of the ice sheet has a positive correlation with the AMO, Camp Century and NW Greenland have a weak negative correlation. This is consistent with the results of Chylek et al. (2012), who found a dominant AMO cycle of 20 years in several ice cores collected from southern and central Greenland, but did not observe an AMO signal in NW Greenland. The positive GIS precipitation correlation with the AMO may be due to warmer North Atlantic and Greenland temperatures

The Cryosphere Discuss., doi:10.5194/tc-2016-248, 2016
Manuscript under review for journal The Cryosphere
Published: 14 November 2016

during AMO positive conditions, leading to higher absolute humidity from the Clausius-Clapeyron relationship (Held and Soden, 2006).

The EOF2 time series is significantly correlated with the wintertime (DJF) North Atlantic Oscillation (NAO), with $r = 0.62$ ($p < 0.03$) for the Hurrell (1995) principle component-based NAO index and $r = 0.60$ ($p < 0.04$) for the Jones et al. (1997) station-based NAO index. Negative correlations in the northern and western regions of our study area are indicative of greater precipitation during NAO negative conditions, when the Icelandic Low and Azores High pressure centers weaken and there is enhanced southerly flow of warm, moist air masses into Baffin Bay (Hurrell, 1995). Banta and McConnell (2007) and Mosley-Thompson et al. (2005) likewise document negative correlations between the NAO and ice core accumulation in central western and northwestern Greenland (e.g. NASA-U, D3, D4; see Figure 2 for locations). Mernild et al. (2014) also find a significant influence of the NAO on their composite coastal Greenland precipitation record, and both Wong et al. (2015) and Osterberg et al., (2015) find significant negative correlations between the NAO and precipitation and temperature, respectively, at Thule in northwest Greenland. The EOF2 loading is also weak in the region of Summit (Figure 10), consistent with the findings of Mosley-Thompson et al. (2005). Interestingly, the EOF2 loading pattern reflects a generally southeast-northwest dipole in accumulation response to the NAO, which differs from the dominantly east-west dipole response to the NAO in reanalysis data (not shown). Varimax rotation of the IceBridge EOF2 did not significantly change the orientation of the dipole.

Using the IceBridge accumulation dataset we can also examine the recent temporal trends in accumulation across the GIS. In most locations the accumulation trend is statistically insignificant from 1712 through the mid-1980s, when accumulation begins to rapidly change across the ice sheet. Thus, we limit this analysis to 1976-2014 to include the entire spatial domain of this dataset (see Figure 2) and to be confident that our accumulation rates are accurately constrained by all the ice cores used to validate study (Table 1).

Figure 10 shows that accumulation is increasing across most of the ice sheet from 1976-2014, with the exception of no significant trend in the north and a negative trend in the northwest. This pattern is almost identical to the EOF1 pattern correlated with the AMO, and thus we hypothesize that rising accumulation over most of the GIS interior since 1976 is related to an increasing AMO index (Mernild et al., 2014). Over the 1981-2012 period, Wong et al. (2015) observed a precipitation decrease of 1.7 mm w.e. decade^{-2} at Camp Century and a precipitation increase of 1.0 mm w.e. decade^{-2} at B26 (see Figure 11 for locations). Over 1976-2014, we also observe a precipitation decrease of 1.08 ± 0.26 mm w.e. decade^{-2} at Camp Century, but a precipitation increase of 0.36 ± 0.097 mm w.e. decade^{-2} at B26.

The Cryosphere Discuss., doi:10.5194/tc-2016-248, 2016
Manuscript under review for journal The Cryosphere
Published: 14 November 2016

The recent increase in accumulation across most of the interior GIS (Figure 11) has partially offset SMB loss from enhanced summer surface melting in recent decades (Sasgen et al., 2012). If our hypothesis is correct that a rising AMO index (warming North Atlantic sea-surface temperatures) contributed to this accumulation increase, then the future behavior of the AMO may have a significant impact on the rate of future GIS mass loss. Hanna et al. (2013) also found that positive AMO summers were associated with enhanced GIS surface melting, indicating that the AMO impacts both the mass input and mass loss portions of the SMB equation in Greenland. Paleoclimate records show evidence of the AMO throughout the late Holocene with a periodicity of 20-70 years (Chylek et al., 2012; Knudsen et al., 2011), and we may be near the peak of the current AMO positive (warm) mode. We recommend future modeling efforts to evaluate the GIS mass balance implications of a return towards AMO negative conditions during a continued rise in radiative forcing from anthropogenic greenhouse gas concentrations.

4. Conclusions

We have developed a new dataset of accumulation rates over the interior of the Greenland ice sheet spanning the past 100-300 years based on 17,730 km of Operation IceBridge airborne Accumulation Radar data. This accumulation record is internally consistent across the dataset and is validated by *in situ* field measurements, several ice cores, and other radar-derived accumulation measurements.

Overall, the Polar MM5, MAR, and RACMO2 Regional Climate Models accurately capture large spatial patterns in accumulation over the GIS, but show significant differences from IceBridge accumulation on a regional basis. For example, MAR overestimates accumulation by as much as 35.5 ± 6.8% in the southeast, while RACMO2 underestimates by 26.9 ± 4.5% in the northern interior of the GIS. These differences could lead to regional Greenland mass balance errors ranging between an underestimate of 42.95 GT a^{-1} and an overestimate of 23.4 GT a^{-1} for the northwest, west, and northeastern drainage basins. These combined regional uncertainties represent up to 12% of the total GIS SMB, and an equivalent of 0.049 to 0.119 mm a^{-1} of less sea level rise than predicted.

Empirical orthogonality function analysis indicates that the first and second principal components explain 33% and 18% percent of the variance and correlate with the AMO and NAO, respectively. These results are consistent with previous ice core and weather station analyses demonstrating the importance of these North Atlantic climate models on Greenland SMB. The increase in accumulation over most of ice sheet between

The Cryosphere Discuss., doi:10.5194/tc-2016-248, 2016
Manuscript under review for journal The Cryosphere
Published: 14 November 2016

1976 and 2014, with no significant trend in the northern interior and a decrease in the northwest, is consistent with the positive AMO trend over this interval. We recommend that future modelling efforts evaluate the effects of a future weakening AMO on GIS surface mass balance as greenhouse gas concentrations continue to rise.

Our largest accumulation uncertainties align with regions that disagree strongest with climate models. Thus, future research should be aimed at collecting additional *in situ* measurements in areas with large disagreement between climate models, particularly in the southeast.

The Cryosphere Discuss., doi:10.5194/tc-2016-248, 2016
Manuscript under review for journal The Cryosphere
Published: 14 November 2016

5. Works cited

Bales, R. C., Guo, Q., Shen, D., McConnell, J. R., Du, G., Burkhart, J. F., Spikes, V. B., Hanna, E. and Cappelen, J.: Annual accumulation for Greenland updated using ice core data developed during 2000-2006 and analysis of daily coastal meteorological data, J. Geophys. Res. Atmos., 114(6), D06116, doi:10.1029/2008JD011208, 2009.

Banta, J. R. and McConnell, J. R.: Annual accumulation over recent centuries at four sites in central Greenland, J. Geophys. Res. Atmos., 112(10), 1–9, doi:10.1029/2006JD007887, 2007.

Box, J. E.: Greenland Ice Sheet Mass Balance Reconstruction. Part II: Surface Mass Balance (1840–2010)*, J. Clim., 26(18), 6974–6989, doi:10.1175/JCLI-D-12-00518.1, 2013.

Box, J. E., Rinke, A., Box, J. E. and Rinke, A.: Evaluation of Greenland Ice Sheet Surface Climate in the HIRHAM Regional Climate Model Using Automatic Weather Station Data, J. Clim., 16, 1302–1319, doi:10.1175/1520-0442-16.9.1302, 2003.

Box, J. E., Bromwich, D. H., Veenhuis, B. a., Bai, L. S., Stroeve, J. C., Rogers, J. C., Steffen, K., Haran, T., Wang, S. H. and Box, Jason E., Bromwich, David H., Veehuis, Bruce A., Bai, Le-Sheng, Strove, Julienne C., Rogers, Jeffrey C., Steffen, Konrad, Haran, T., Wang, S.-H.: Greenland Ice Sheet Surface Mass Balance Variability (1988 – 2004) from Calibrated Polar MM5 Output *, J. Clim., 19(12), 2783–2801, doi:doi.org/10.1175/JCLI3738.1, 2006.

van den Broeke, M. R., Bamber, J. L., Ettema, J., Rignot, E. J., Schrama, E., van de Berg, W. J., van Meijgaard, E., Velicogna, I. and Wouters, B.: Partitioning recent Greenland mass loss., Science, 326(5955), 984–6, doi:10.1126/science.1178176, 2009.

Burgess, E. W., Forster, R. R., Box, J. E., Mosley-Thompson, E., Bromwich, D. H., Bales, R. C. and Smith, L. C.: A spatially calibrated model of annual accumulation rate on the Greenland Ice Sheet (1958-2007), J. Geophys. Res. Earth Surf., 115(2), 1–14, doi:10.1029/2009JF001293, 2010.

Chylek, P., Folland, C., Frankcombe, L., Dijkstra, H., Lesins, G. and Dubey, M.: Greenland ice core evidence for spatial and temporal variability of the Atlantic Multidecadal Oscillation, Geophys. Res. Lett., 39(9), 1–6, doi:10.1029/2012GL051241, 2012.

Cole-Dai, J., Ferris, D., Lanciki, A., Savarino, J., Baroni, M. and Thiemens, M. H.: Cold decade (AD 1810-1819) caused by Tambora (1815) and another (1809) stratospheric volcanic eruption, Geophys. Res. Lett., 36(22), 1–6, doi:10.1029/2009GL040882, 2009.

Déry, S. J. and Yau, M. K.: Large-scale mass balance effects of blowing snow and surface sublimation, J.

Geophys. Res. Atmos., 107(23), doi:10.1029/2001JD001251, 2002.

Dumont, M., Brun, E., Picard, G., Michou, M., Libois, Q., Petit, J., Geyer, M., Morin, S. and Josse, B.: Contribution of light-absorbing impurities in snow to Greenland's darkening since 2009, Nat. Geosci., 7(7), 509–512, doi:10.1038/ngeo2180, 2014.

Ettema, J., van den Broeke, M. R., van Meijgaard, E., van de Berg, W. J., Bamber, J. L., Box, J. E. and Bales, R. C.: Higher surface mass balance of the Greenland ice sheet revealed by high-resolution climate modeling, Geophys. Res. Lett., 36(12), L12501, doi:10.1029/2009GL038110, 2009.

Fettweis, X., Franco, B., Tedesco, M., van Angelen, J. H., Lenaerts, J. T. M., van den Broeke, M. R. and Gallée, H.: Estimating Greenland ice sheet surface mass balance contribution to future sea level rise using the regional atmospheric climate model MAR, Cryosph., 7, 469–489, doi:10.5194/tcd-6-3101-2012, 2012.

Fischer, H., Wagenbach, D., Laternser, M. and Haeberli, W.: Glacio-meteorological and isotopic studies along the EGIG line, central Greenland, J. Glaciol., 41(139), 515–527, 1995.

Hall, D. K., Comiso, J. C., DiGirolamo, N. E., Shuman, C. A., Key, J. R. and Koenig, L. S.: A satellite-derived climate-quality data record of the clear-sky surface temperature of the Greenland ice sheet, J. Clim., 25(14), 4785–4798, 2012.

Hanna, E., Navarro, F. J., Pattyn, F., Domingues, C. M., Fettweis, X., Ivins, E. R., Nicholls, R. J., Ritz, C., Smith, B., Tulaczyk, S., Whitehouse, P. L. and Zwally, H. J.: Ice-sheet mass balance and climate change., Nature, 498(7452), 51–9, doi:10.1038/nature12238, 2013.

Hawley, R. L., Courville, Z. R., Kehrl, L. M., Lutz, E. R., Osterberg, E. C., Overly, T. B. and Wong, G. J.: Recent accumulation variability in northwest Greenland from ground-penetrating radar and shallow cores along the Greenland Inland Traverse, J. Glaciol., 60(220), 375–382, doi:10.3189/2014JoG13J141, 2014.

Held, I. M. and Soden, B. J.: Robust responses of the hydrological cycle to global warming, J. Clim., 19(21), 5686–5699, doi:10.1175/JCLI3990.1, 2006.

Helm, V., Humbert, A. and Miller, H.: Elevation and elevation change of Greenland and Antarctica derived from CryoSat-2, Cryosph. Discuss., 8(2), 1673–1721, doi:10.5194/tcd-8-1673-2014, 2014.

Herron, M. M. and Langway, C. C.: Firn densification: an empirical model., J. Glaciol., 25(93), 373–385, doi:10.3198/1980JoG25-93-373-385, 1980.

Hurrell, J. W.: Decadal Trends in the North Atlantic Oscillation: Regional Temperatures and Precipitation., Science, 269(5224), 676–9, doi:10.1126/science.269.5224.676, 1995.

IPCC: Summary for Policymakers, in Climate Change 2014: Impacts, Adaptation, and Vulnerability. Part A: Global and Sectoral Aspects. Contribution of Working Group II to the Fifth Assessment Report of the Intergovernmental Panel on Climate Change, edited by C. B. Field, V. R. Barros, D. J.

Dokken, K. J. Mach, M. D. Mastrandrea, T. E. Bilir, M. Chatterjee, K. L. Ebi, Y. O. Estrada, R. C. Genova, B. Girma, E. S. Kissel, A. N. Levy, S. MacCracken, P. R. Mastrandrea, and L. L. White, pp. 1–32, Cambridge University Press, Cambridge, United Kingdom, and New York, NY, USA., 2014.

Jones, P. D., Jonsson, T. and Wheeler, D.: Extension to the North Atlantic oscillation using early instrumental pressure observations from Gibraltar and south-west Iceland, Int. J. Climatol., 17(13), 1433–1450, doi:10.1002/(SICI)1097-0088(19971115)17:13<1433::AID-JOC203>3.0.CO;2-P, 1997.

Karlöf, L., Isaksson, E., Winther, J. G., Gundestrup, N., Meijer, H. A. J., Mulvaney, R., Pourchet, M., Hofstede, C., Lappegard, G., Petterson, R., van den Broeke, M. and van de Wal, R. S. W.: Accumulation variability over a small area in east Dronning Maud Land, Antarctic, as determined from shallow firn cores and snow pits: Some implications for ice-core records, J. Glaciol., 51(174), 343–352, doi:10.3189/172756505781829232, 2005.

Khan, S. A., Aschwanden, A., Bjørk, A. A., Wahr, J., Kjeldsen, K. K. and Kjaer, K. H.: Greenland ice sheet mass balance: a review, Reports Prog. Phys., 46801, 1–26, doi:10.1088/0034-4885/78/4/046801, 2015.

Knudsen, M. F., Seidenkrantz, M.-S., Jacobsen, B. H. and Kuijpers, A.: Tracking the Atlantic Multidecadal Oscillation through the last 8,000 years., Nat. Commun., 2, 178, doi:10.1038/ncomms1186, 2011.

Koenig, L. S., Ivanoff, A., Alexander, P. M., MacGregor, J. A., Fettweis, X., Panzer, B., Paden, J. D., Forster, R. R., Das, I., McConnell, J. R., Tedesco, M., Leuschen, C. and Gogineni, P.: Annual Greenland accumulation rates (2009–2012) from airborne snow radar, Cryosph., 10(4), 1739–1752, doi:10.5194/tc-10-1739-2016, 2016.

Kovacs, A., Gow, A. J. and Morey, R. M.: The in-situ dielectric constant of polar firn revisited, Cold Reg. Sci. Technol., 23(3), 245–256, doi:10.1016/0165-232X(94)00016-Q, 1995.

Leuschen, C., Lewis, C., Gogineni, S. P., Rodriguez-Morales, F., Paden, J. D. and Li, J.: IceBridge Accumulation Radar L1B Geolocated Radar Echo Strength Profiles, Boulder, Color. USA Natl. Snow Ice Data Center. Digit. media, 2011.

McConnell, J. R., Arthern, R., Mosley-Thompson, E., Davis, C., Bales, R. C., Thomas, R., Burkhart, J. and Kyne, J.: Changes in Greenland ice sheet elevation attributed primarily to snow accumulation variability, Nature, 406(6798), 877–9, doi:10.1038/35022555, 2000.

McGrath, D., Colgan, W., Bayou, N., Muto, A. and Steffen, K.: Recent warming at Summit, Greenland: Global context and implications, Geophys. Res. Lett., 40(10), 2091–2096, doi:10.1002/grl.50456, 2013.

Medley, B., Joughin, I., Das, S. B., Steig, E. J., Conway, H., Gogineni, S. P., Criscitiello, a. S., McConnell,

J. R., Smith, B. E., van den Broeke, M. R., Lenaerts, J. T. M., Bromwich, D. H. and Nicolas, J. P.: Airborne-radar and ice-core observations of annual snow accumulation over Thwaites Glacier, West Antarctica confirm the spatiotemporal variability of global and regional atmospheric models, Geophys. Res. Lett., 40(14), 3649–3654, doi:10.1002/grl.50706, 2013.

Mernild, S. H., Hanna, E., Mcconnell, J. R., Sigl, M., Beckerman, A. P., Yde, J. C., Cappelen, J., Malmros, J. K. and Steffen, K.: Greenland precipitation trends in a long-term instrumental climate context (1890-2012): Evaluation of coastal and ice core records, Int. J. Climatol., doi:10.1002/joc.3986, 2014.

Miège, C., Forster, R. R., Box, J. E., Burgess, E. W., McConnell, J. R., Pasteris, D. R. and Spikes, V. B.: Southeast Greenland high accumulation rates derived from firn cores and ground-penetrating radar, Ann. Glaciol., 54(63), 322–332, doi:10.3189/2013AoG63A358, 2013.

Mosley-Thompson, E., McConnell, J. R., Bales, R. C., Li, Z., Lin, P.-N., Steffen, K., Thompson, L. G., Edwards, R. and Bathke, D.: Local to regional-scale variability of annual net accumulation on the Greenland ice sheet from PARCA cores, J. Geophys. Res., 106(D24), 33839, doi:10.1029/2001JD900067, 2001.

Mosley-Thompson, E., Readinger, C. R., Craigmile, P., Thompson, L. G. and Calder, C. A.: Regional sensitivity of Greenland precipitation to NAO variability, Geophys. Res. Lett., 32(24), 1–4, doi:10.1029/2005GL024776, 2005.

Osterberg, E. C., Hawley, R. L., Wong, G., Kopec, B., Ferris, D. and Howley, J.: Coastal ice-core record of recent northwest Greenland temperature and sea-ice concentration, J. Glaciol., 61(230), 1137–1146, doi:10.3189/2015JoG15J054, 2015.

Overly, T. B., Hawley, R. L., Helm, V., Morris, E. M. and Chaudhary, R. N.: Greenland annual accumulation along the EGIG line, 1959–2004, from ASIRAS airborne radar and neutron-probe density measurements, Cryosph., 10(4), 1679–1694, doi:10.5194/tc-10-1679-2016, 2016.

Rodriguez-Morales, F., Gogineni, S. P., Leuschen, C. J., Paden, J. D., Li, J., Lewis, C. C., Panzer, B., Gomez-Garcia Alvestegui, D., Patel, A., Byers, K., Crowe, R., Player, K., Hale, R. D., Arnold, E. J., Smith, L., Gifford, C. M., Braaten, D. and Panton, C.: Advanced multifrequency radar instrumentation for polar Research, IEEE Trans. Geosci. Remote Sens., 52(5), 2824–2842, doi:10.1109/TGRS.2013.2266415, 2014.

Sasgen, I., van den Broeke, M. R., Bamber, J. L., Rignot, E., Sorensen, L. S., Wouters, B., Martinec, Z., Velicogna, I. and Simonsen, S. B.: Timing and origin of recent regional ice-mass loss in Greenland, Earth Planet. Sci. Lett., 333–334, 293–303, doi:10.1016/j.epsl.2012.03.033, 2012.

Shepherd, A.: A reconciled estimate of ice sheet mass balance, Science (80-.)., 338(November), 1183–1189 [online] Available from: http://dx.doi.org/10.1126/science.1228102, 2012.

Spikes, V. B., Hamilton, G. S., Arcone, S. A., Kaspari, S. and Mayewski, P. A.: Variability in accumulation rates from GPR profiling on the West Antarctic plateau, Ann. Glaciol., 39, 238–244, doi:10.3189/172756404781814393, 2004.

Vernon, C. L., Bamber, J. L., Box, J. E., Van Den Broeke, M. R., Fettweis, X., Hanna, E. and Huybrechts, P.: Surface mass balance model intercomparison for the Greenland ice sheet, Cryosph., 7(5), 599–614, doi:10.5194/tc-7-599-2013, 2013.

Wong, G. J., Osterberg, E. C., Hawley, R. L., Courville, Z. R., Ferris, D. G. and Howley, J. A.: Coast-to-interior gradient in recent northwest Greenland precipitation trends (1952 – 2012), Environ. Res. Lett., 10(11), 114008, doi:10.1088/1748-9326/10/11/114008, 2015.

The Cryosphere Discuss., doi:10.5194/tc-2016-248, 2016
Manuscript under review for journal The Cryosphere
Published: 14 November 2016

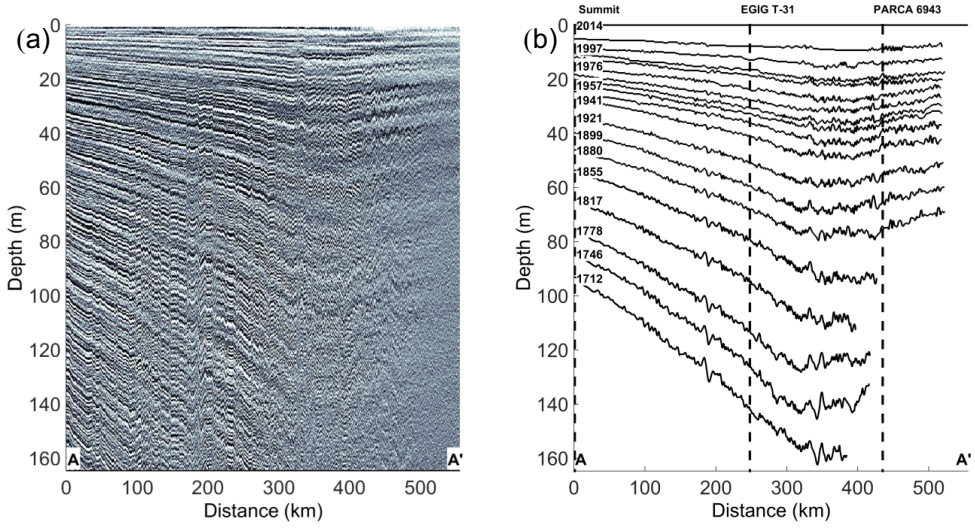

Figure 1: a) Radargram showing flight A-A' (see Figure 2 for location). b) Nineteen traced internal reflecting horizons from two dated ice cores at Summit Station through EGIG T-31 and PARCA 6943 ice cores.

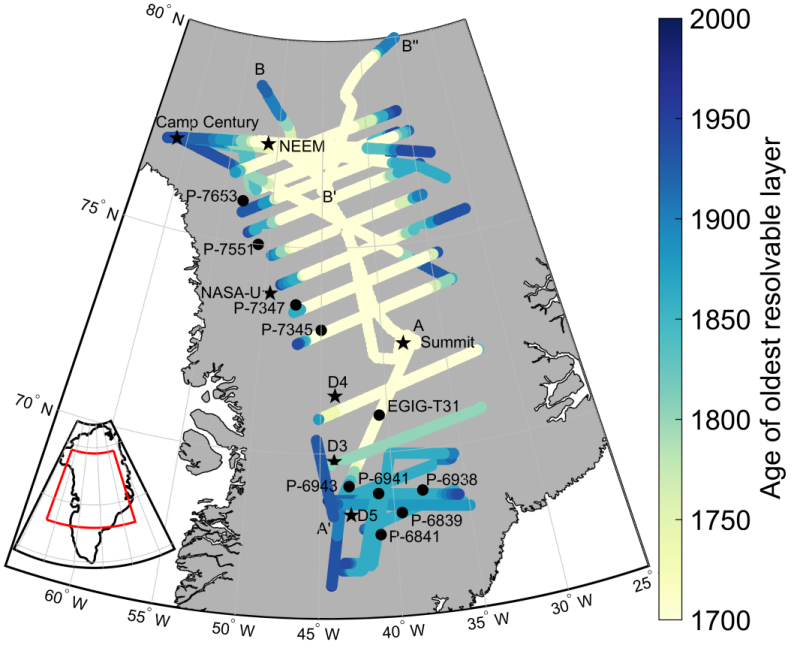

Figure 2: Age of oldest resolvable layer along 25 IceBridge Accumulation Radar flights totaling 17,730 km. Locations are shown for A-A' (Figure 1) and B'-B'-B'' (Figure 7) as well as the EGIG-T31 and D3, D4, D5, NEEM, NASA-U, Camp Century, and PARCA ice cores (Figure 5 and Table 1).

The Cryosphere Discuss., doi:10.5194/tc-2016-248, 2016
Manuscript under review for journal The Cryosphere
Published: 14 November 2016

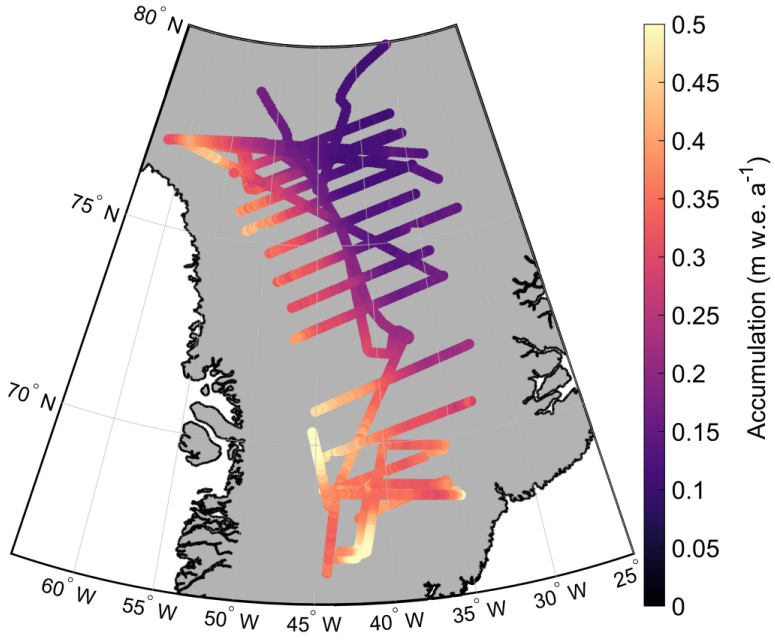

Figure 3. Average accumulation from 1712-2014 AD calculated from IceBridge Accumulation Radar over all 25 flights. IceBridge accumulation matches large-scale accumulation patterns from ice cores and snow pits.

The Cryosphere Discuss., doi:10.5194/tc-2016-248, 2016
Manuscript under review for journal The Cryosphere
Published: 14 November 2016

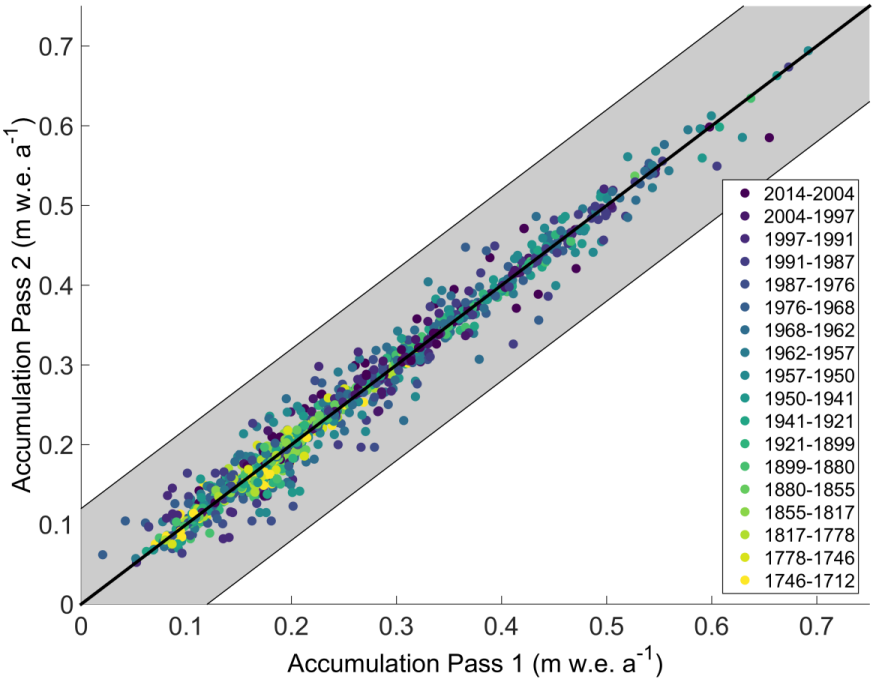

Figure 4. Comparison of IceBridge accumulation rates determined at 87 crossover locations for each epoch, totaling 1272 measurements. There are no temporal or spatial patterns in crossover location accumulation differences. Shaded region is the calculated uncertainty of ±0.127 m w.e. a^{-1}.

5

The Cryosphere Discuss., doi:10.5194/tc-2016-248, 2016
Manuscript under review for journal The Cryosphere
Published: 14 November 2016

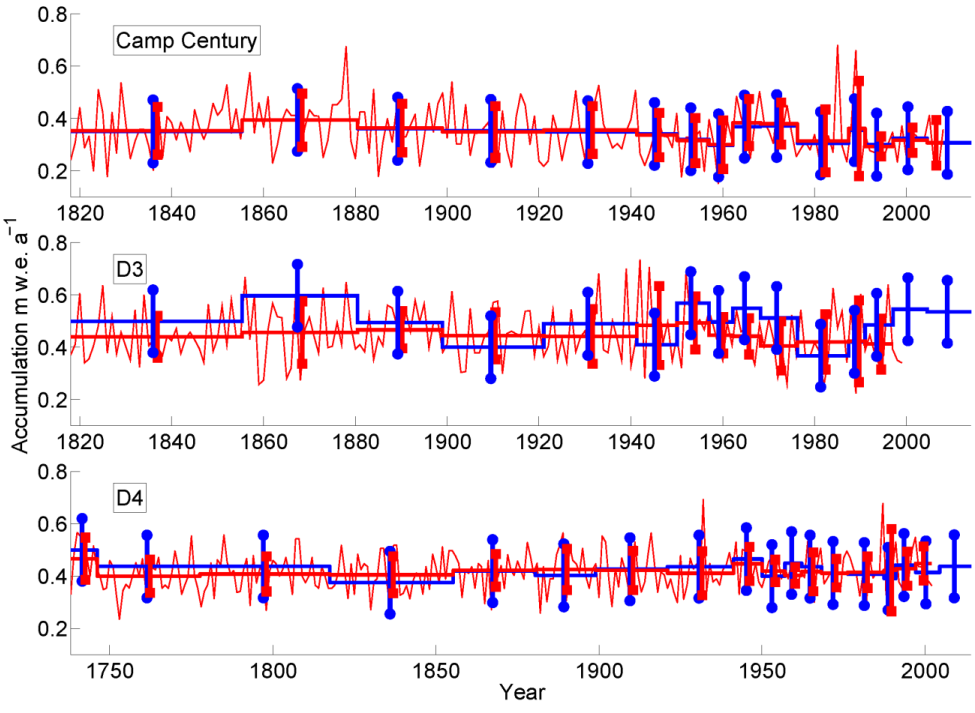

Figure 5. IceBridge accumulation (blue) with uncertainty (blue circles) compared with Camp Century, D3, and D4 (see Figure 2 for locations) ice core annual accumulation (thin red lines) and ice core accumulation averaged over corresponding epochs (thick red lines). One standard deviation of ice core annual accumulation over each epoch is shown with a red square. Note the longer time scale for the D4 ice core. There is no statistically significant difference between IceBridge and ice core accumulation for any of these ice cores.

The Cryosphere Discuss., doi:10.5194/tc-2016-248, 2016
Manuscript under review for journal The Cryosphere
Published: 14 November 2016

Table 1. Averaged ice core accumulation compared with IceBridge accumulation averaged over the time domain of each ice core.

Ice Core	Average Ice Core Accumulation (m w.e. a^{-1})	Average IceBridge Accumulation (m w.e. a^{-1})
Nasa-U	0.35 ± 0.08	0.35 ± 0.04
NEEM	0.19 ± 0.04	0.21 ± 0.07
Camp Century	0.35 ± 0.1	0.34 ± 0.03
D3	0.45 ± 0.1	0.49 ± 0.07
D4	0.42 ± 0.07	0.43 ± 0.03
D5	0.35 ± 0.08	0.37 ± 0.04
P-6839	0.39 ± 0.15	0.38 ± 0.08
P-6841	0.48 ± 0.16	0.45 ± 0.03
P-6938	0.36 ± 0.07	0.33 ± 0.05
P-6941	0.4 ± 0.1	0.4 ± 0.03
P-6943	0.39 ± 0.1	0.39 ± 0.06
P-7345	0.28 ± 0.07	0.33 ± 0.07
P-7347	0.29 ± 0.09	0.33 ± 0.09
P-7551	0.32 ± 0.09	0.32 ± 0.12
P-7653	0.35 ± 0.09	0.34 ± 0.05

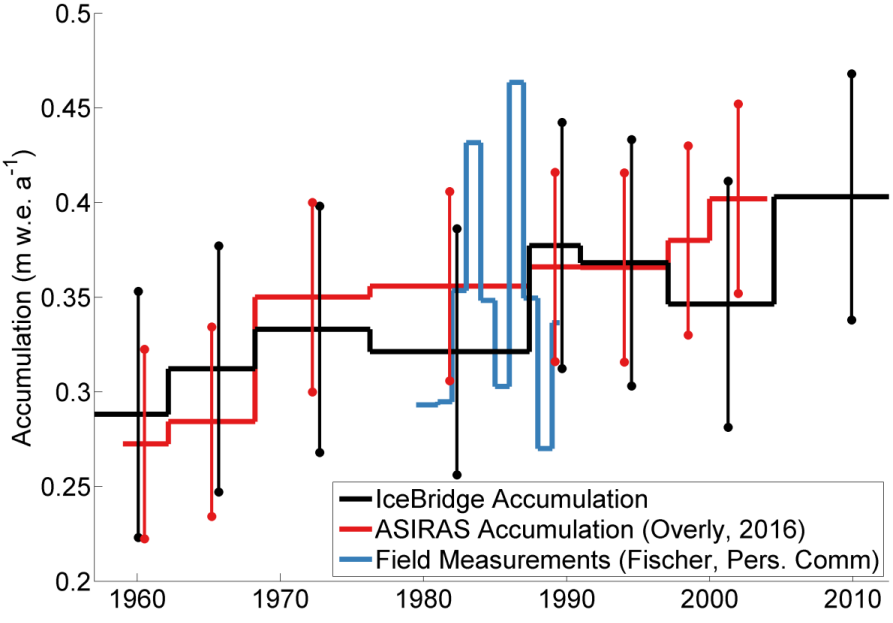

Figure 6: IceBridge accumulation results at EGIG T-31 (see Figure 2 for locations) from 1957-2014 are statistically indistinguishable from Airborne SAR/Interferometric Radar Altimeter System (ASIRAS) accumulation (Overly et al., 2016), and field measurements (H. Fischer, personal communication, 2015). Error bars are 1 standard deviation of ASIRAS accumulation over data points from that time period.

The Cryosphere Discuss., doi:10.5194/tc-2016-248, 2016
Manuscript under review for journal The Cryosphere
Published: 14 November 2016

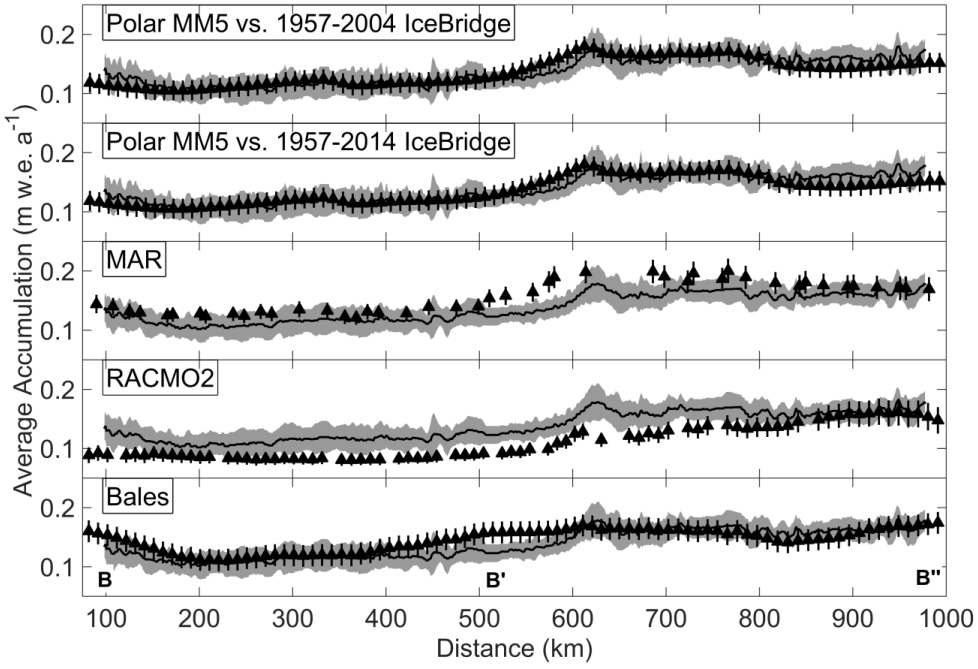

Figure 7: Comparison of 1957-2004 averaged IceBridge accumulation (solid line) and uncertainty (shaded region) to averaged Polar MM5 (1958-2008; triangles) along a 977 km flight in northern Greenland. Location of flight shown as B-B'-B'' on Figure 2. Comparison of 1957-2014 averaged IceBridge accumulation to averaged Polar MM5 (1957-2008), MAR (1958-2013), RACMO2 (1958-2014), and Bales09 accumulation along the same flight. The difference between 1957-2004 and 1957-2014 IceBridge accumulation across this flight is insignificant.

The Cryosphere Discuss., doi:10.5194/tc-2016-248, 2016
Manuscript under review for journal The Cryosphere
Published: 14 November 2016

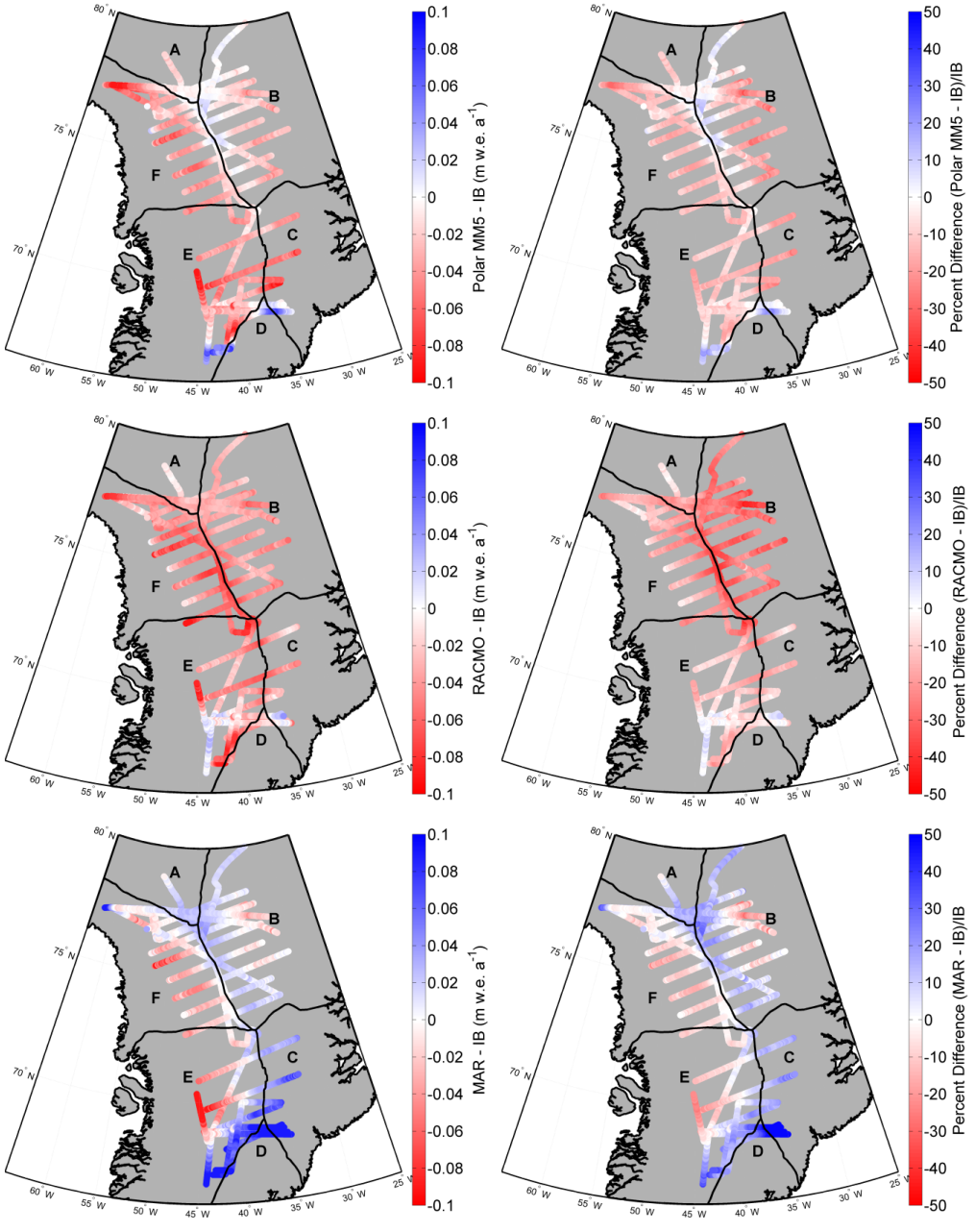

Figure 8. Magnitude (left) and percent (right) differences between averaged 1957-2014 IceBridge accumulation and Polar MM5 (top), RACMO2 (middle), and MAR (bottom) averaged accumulation. Polar MM5 underestimates in the NW and overestimates in the southeast, RACMO2 underestimates across this dataset, and MAR overestimates in the SE. Also shown are six drainage basins of the Greenland Ice Sheet discussed in the text (c.f. Vernon et al., 2013).

The Cryosphere Discuss., doi:10.5194/tc-2016-248, 2016
Manuscript under review for journal The Cryosphere
Published: 14 November 2016

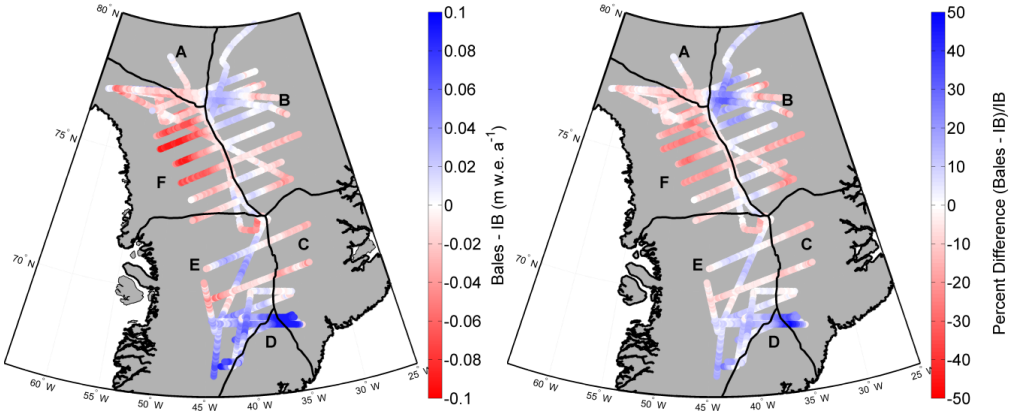

Figure 9. Magnitude (left) and percent differences (right) between averaged 1957-2014 IceBridge accumulation and Bales09 accumulation. Bales09 does not significantly differ from IceBridge accumulation in any drainage basin.

5

The Cryosphere Discuss., doi:10.5194/tc-2016-248, 2016
Manuscript under review for journal The Cryosphere
Published: 14 November 2016

Table 2. Percent and magnitude differences between average 1957-2014 IceBridge accumulation and average model accumulation in each of the six Greenland Ice Sheet drainage basins. Positive numbers indicate that the model overestimates accumulation in that basin. Statistically significant differences are indicated in bold.

	A (n = 135)	B (n = 815)	C (n = 234)	D (n = 102)	E (n = 1064)	F (n = 831)
Polar MM5 (%)	-2.59 ± 3.73	-7.40 ± 7.95	**-8.92 ± 3.74**	4.52 ± 5.85	-8.04 ± 4.88	**-11.00 ± 5.24**
RACMO2 (%)	**-15.02 ± 3.97**	**-26.88 ± 4.48**	-7.69 ± 5.07	**-10.13 ± 1.93**	-8.38 ± 5.76	**-17.71 ± 6.42**
MAR (%)	**14.30 ± 4.70**	6.55 ± 8.81	**35.51 ± 6.80**	**27.60 ± 9.19**	3.91 ± 8.50	-1.51 ± 6.24
Bales09 (%)	-4.13 ± 4.68	3.63 ± 9.20	6.36 ± 5.22	16.91 ± 8.74	4.68 ± 4.88	-8.76 ± 5.20
Polar MM5 (m w.e. a^{-1})	-0.004 ± 0.006	-0.010 ± 0.011	**-0.026 ± 0.011**	0.016 ± 0.022	-0.031 ± 0.021	**-0.035 ± 0.019**
RACMO2 (m w.e. a^{-1})	**-0.026 ± 0.008**	**-0.036 ± 0.009**	-0.021 ± 0.016	**-0.038 ± 0.009**	-0.031 ± 0.021	**-0.048 ± 0.014**
MAR (m w.e. a^{-1})	**0.023 ± 0.007**	0.009 ± 0.013	**0.119 ± 0.027**	**0.098 ± 0.027**	0.010 ± 0.033	-0.007 ± 0.018
Bales09 (m w.e. a^{-1})	-0.007 ± 0.008	0.003 ± 0.012	0.025 ± 0.015	0.059 ± 0.028	0.016 ± 0.018	-0.027 ± 0.017

The Cryosphere Discuss., doi:10.5194/tc-2016-248, 2016
Manuscript under review for journal The Cryosphere
Published: 14 November 2016

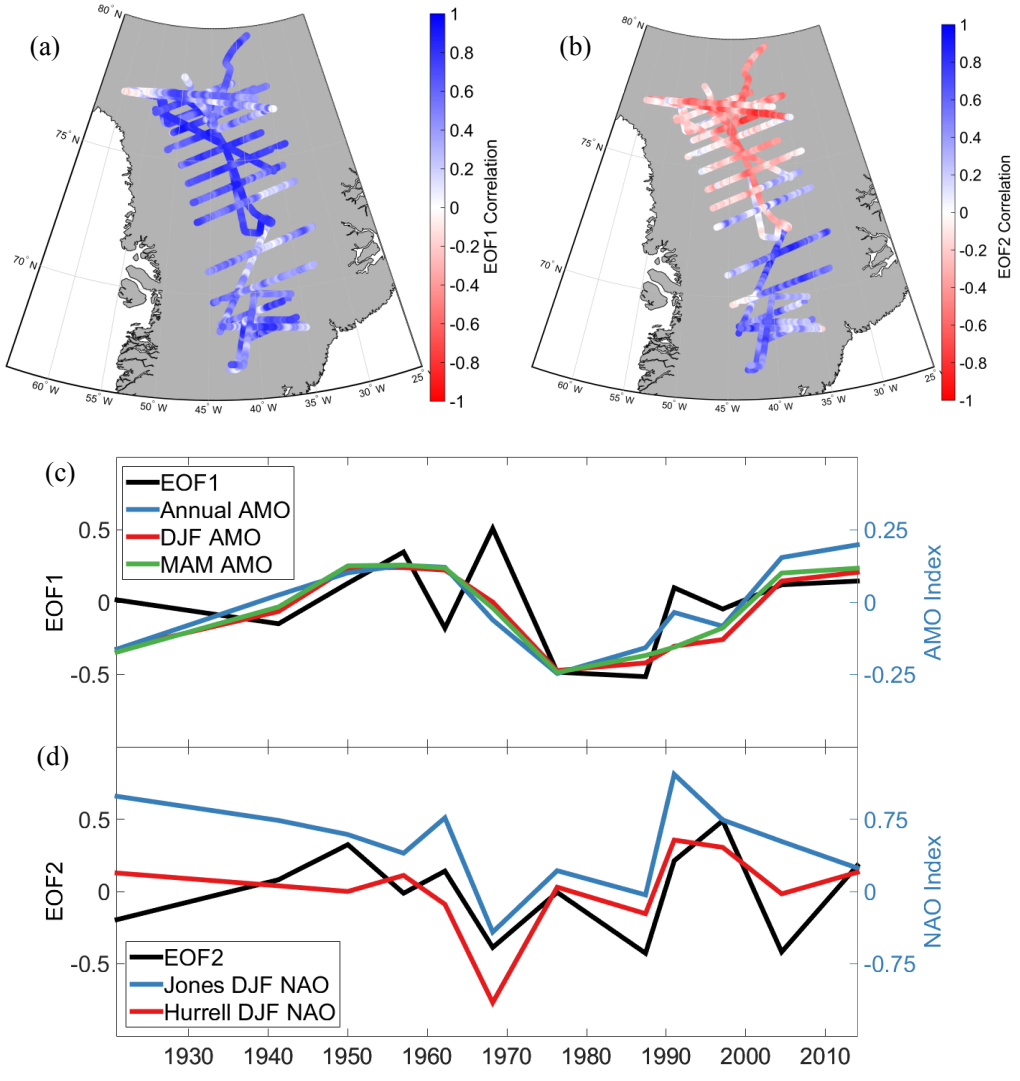

Figure 10: Map of correlation between IceBridge accumulation and a) EOF1 and b) EOF2. c) EOF1 time series compared with the annually averaged, wintertime, and springtime Atlantic Meridional Oscillation (AMO) indices. d) EOF2 compared with the wintertime Hurrell (1995) and Jones (1997) North Atlantic Oscillation (NAO) indices.

The Cryosphere Discuss., doi:10.5194/tc-2016-248, 2016
Manuscript under review for journal The Cryosphere
Published: 14 November 2016

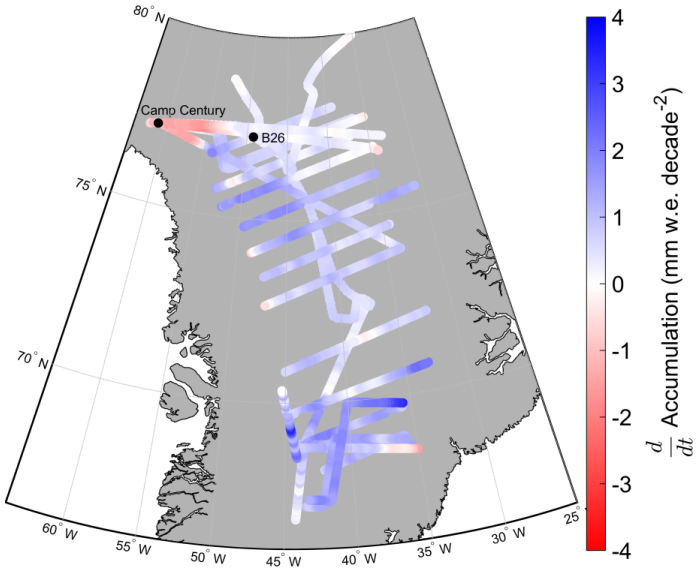

Figure 11: Accumulation trend from 1976-2014 across all 25 IceBridge flights. Accumulation has increased across most of the Greenland Ice Sheet, with no significant trend in the north and a decrease in the northwest.